Biomaterials Processing

JOURNAL OF
biomaterials applications

Journal of Biomaterials Applications
2016, Vol. 30(9) 1362–1372

DOI: 10.1177/0885328215626361
jba.sagepub.com
SAGE

Preparation and bioactive properties of nano bioactive glass and segmented polyurethane composites

Fernando J Aguilar-Pérez[1,2], Rossana F Vargas-Coronado[1], Jose M Cervantes-Uc[1], Juan V Cauich-Rodríguez[1], Cristian Covarrubias[3] and Merhdad Pedram-Yazdani[4]

Abstract

Composites of glutamine-based segmented polyurethanes with 5 to 25 wt.% bioactive glass nanoparticles were prepared, characterized, and their mineralization potential was evaluated in simulated body fluid. Biocompatibility with dental pulp stem cells was assessed by MTS to an extended range of compositions (1 to 25 wt.% of bioactive glass nanoparticles). Physicochemical characterization showed that composites retained many of the matrix properties, i.e. those corresponding to semicrystalline elastomeric polymers as they exhibited a glass transition temperature (T_g) between −41 and −36°C and a melting temperature (T_m) between 46 and 49°C in agreement with X-ray reflections at 23.6° and 21.3°. However, with bioactive glass nanoparticles addition, tensile strength and strain were reduced from 22.2 to 12.2 MPa and 667.2 to 457.8%, respectively with 25 wt.% of bioactive glass nanoparticles. Although Fourier transform infrared spectroscopy did not show evidence of mineralization after conditioning of these composites in simulated body fluid, X-ray diffraction, scanning electron microscopy, and energy dispersive X-ray microanalysis showed the formation of an apatite layer on the surface which increased with higher bioactive glass concentrations and longer conditioning time. Dental pulp stem cells proliferation at day 5 was improved in bioactive glass nanoparticles composites containing lower amounts of the filler (1–2.5 wt.%) but it was compromised at day 9 in composites containing high contents of nBG (5, 15, 25 wt.%). However, Runx2 gene expression was particularly upregulated for the dental pulp stem cells cultured with composites loaded with 15 and 25 wt.% of bioactive glass nanoparticles. In conclusion, low content bioactive glass nanoparticles and segmented polyurethanes composites deserve further investigation for applications such as guided bone regeneration membranes, where osteoconductivity is desirable but not a demanding mechanical performance.

Keywords

Segmented polyurethane, nanobioactive glass, bone regeneration, mineralization

Introduction

Bone loss can occur for numerous reasons including trauma, cancer, osteomyelitis, and periodontal disease that generates bone defects of varying sizes and locations in the body. Hence, there is an increasing need for bone grafts in the field of orthopaedics, maxillofacial surgery and dentistry, which in the case of periodontal disease, affects 92% of world population according to World Health Organization (WHO).[1] Since the use of autologous graft is not always possible due to the scarcity of bone tissue or difficulties in shaping it into a specific geometry, a possible solution is to provide biomaterials able to enhance the body's own repair ability.[2]

The ideal material for bone regeneration therefore must exhibit a controlled biodegradability, open and highly interconnected porosity (macro and micro), bone cell proliferation, mechanical properties similar to trabecular or cortical bone, biocompatibility, long

[1]Unidad de Materiales, Centro de Investigación Científica de Yucatán, Merida, México
[2]Facultad de Odontología, Universidad Autónoma de Yucatán, Merida, México
[3]Laboratorio de Nanobiomateriales, Facultad de Odontología, Universidad de Chile, Santiago, Chile
[4]Facultad de Ciencias Químicas y Farmacéuticas, Universidad de Chile, Santiago, Chile

Corresponding author:
Juan V Cauich-Rodríguez, Unidad de Materiales, Centro de Investigación Científica de Yucatán, Calle 43 130, Colonia Chuburná de Hidalgo, C.P. 97200, Mérida, Yucatán, México.
Email: jvcr@cicy.mx

storage life, and ease of sterilization.[3,4] Although these requirements are very complex and demanding, they can be fulfilled by a versatile family of polymers known as polyurethanes (PU).[5] In the case of segmented PUs, biodegradation can be controlled by incorporating biodegradable soft segments (PCL)[6] or labile linkages in the rigid segment (lysine ester diisocyanate, 1,4-diisocyanatebutane tyramine, etc.), while their mechanical properties can be tailored by incorporating various types of bioactive fillers, like hydroxyapatite (HA),[7] β-tricalcium phosphate (β-TCP),[8] and various bioactive glasses.[9,10]

Bioactive glasses (BGs) are reported to stimulate more bone regeneration than any other bioactive ceramic and even to promote angiogenesis.[11] Upon implantation, BGs gradually convert to HA or carbonated hydroxyapatite (HCA), which chemically bond to the underlying bone, the main mineral constituent of bone.[9] The growing HCA layer provides an ideal environment for colonization by osteoblast bone-forming cells followed by proliferation and differentiation of the cells to form new bone.[12] BG stimulates cell proliferation and the upregulation of genes known to be involved in osteoblast metabolism and bone homeostasis.[13]

In spite of these advantages, BGs cannot share the load with the bone, as they are brittle.[4] One way to improve this behavior is to use them as hybrids or composites within a polymeric matrix. Literature reports that foams of PU/BG composite can be manufactured with porosities greater than 60%, interconnected pores >100 μm,[9] and that the composite foams had higher elastic modulus than the pure PU foams. High bioactivity of PU/BG composite was confirmed based on the behavior of these materials in simulated body fluid (SBF), which led to the formation of HA on the surface of the foam.[9] Therefore, it is clear that BG addition can improve the performance of these composites but it is also clear that BG is commonly incorporated into polymeric matrices by using microsized particles.[9,11,14,15] However, the advances in sol-gel technique enable the production of BG with nanometric particle size, which exhibits improved bioactivity accelerating the crystallization of the HA layer as well as the cell differentiation process.[12,16]

De Oliveira et al.[10] reported segmented PU foams with up to 10% of bioactive glass nanoparticles that act as reinforcement to improve their mechanical properties, specifically increasing its elastic modulus. Although the mechanical properties of these composites are still below the mechanical properties of cancellous bone they can meet the requirements necessary to support growth and cell proliferation as these materials formed a layer of HA after an immersion in SBF. An additional relevant feature of these foams was their ease for surgical management, as they can be anatomically adapted to the shape of the implantation site.[10]

Previous studies of our group have shown that segmented PU prepared with glutamine (GLU) were less biocompatible compared to other PU prepared with other biologically important molecules.[17] This was explained by a higher GLU release than required by human alveolar osteoblasts and even ammonia production. Therefore, it is hypothesized that the properties of GLU-based PU can be improved by the addition of bioactive glass nanoparticles (nBG), producing thus a composite enable able to stimulate HA formation and cellular activity.

In this work, segmented PUs based on L-GLU as chain extender were synthesized and composites prepared with varying amounts of nBG. These composites were conditioned in SBF and their mineralization potential followed by FTIR, EDX, XRD, and SEM. The cytocompatibility and cell differentiation properties of the materials were preliminarily assessed using dental pulp stem cells (DPSC).

Materials and methods

Synthesis of bioactive glass nanoparticles (nBG)

Nanosized BG particles were synthesized by the sol-gel method following the procedure reported previously.[12] The synthesis mixture (molar composition: $58SiO_2$: $40CaO$:$5P_2O_5$) was stirred for 48 h and aged for 48 h at room temperature. The precipitate was separated by centrifugation (12,000 r/min) and washed by three centrifugation-redispersion cycles with distilled water, freeze dried, and then calcined at 700°C for 3 h to obtain a fine white nBG powder. The particle size was measured by Dynamic Light Scattering (DLS) using a Malvern Zetasizer Nano ZEN3600 and by scanning electron microscopy (SEM) with a JEOL, JMS 6360LV.

PU synthesis

A segmented PU with GLU (SPU-G) was synthesized by two-step polymerization method, using polycaprolactone diol (PCL) as soft segment, and 4,4-methylene-bis ciclohexyl diisocyanate (HMDI) and GLU as chain extender for rigid segment formation. In the first stage, PCL was dissolved in anhydrous DMF and then an excess of HMDI was slowly added in the presence of 0.3% of stannous octoate during 4 h at 60°C. In the second step, GLU was added and left to react during 2 h more. The SPU-G was precipitated in water and washed several times before drying at 60°C during 24 h. Films of neat SPU-G for the different characterizations were obtained after chloroform evaporation.

Figure 1 shows the suggested structure for the synthesized SPU-G with a 1:2.05:1.05 molar ratio (PCL: HMDI:GLU).

Composite preparation

Composites with nBG were prepared dispersing the proper amount of glass particles in chloroform and then adding this suspension to a SPU-G chloroform solution. The suspension was sonicated during 30 min and then poured in a Teflon mold. After evaporation at 25°C for a minimum of 24 h, films of the composites were obtained. With this procedure, composites with 5, 15, and 25 wt.% were prepared.

Composite physicochemical and mechanical characterization

Infrared spectroscopy (FTIR). Fourier transform infrared spectroscopy (FTIR) spectra were obtained using attenuated total reflectance (ATR) in the 4000 and 650 cm^{-1} spectral range averaging 50 scans with a resolution of 4 cm^{-1}. For this, a Thermo Scientific Nicolet 8700 spectrometer was used.

Differential scanning calorimetry. Melting point (Tm) was determined with a Perkin Elmer DSC-7, using 5–7 mg of the composite, after heating from −5 to 150°C with a heating rate of 10°C/min under nitrogen atmosphere.

Thermogravimetric analysis. Mass loss was obtained with 25 mg of the sample after heating from 50 to 650°C at 10°C/min under nitrogen atmosphere by means of a TGA-7 from Perkin Elmer. From the mass loss first derivative, the decomposition temperature (T_d) was obtained.

Dynamic mechanical analysis. Storage modulus (E′) and the dissipation factor (Tan δ) were obtained with a Perkin Elmer DMA-7. For this, rectangular samples of 20 mm long, 4 mm wide, and 0.1 mm thickness were deformed in the extension mode with a static load of 80 mN and a dynamic load of 65 mN at frequency of 1 Hz while heated from −100 to 75°C at 5°C/min.

X-ray diffraction. Crystallinity was confirmed by X-ray diffraction (XRD) using a Siemens D5000 diffractometer with radiation CuKα ($\lambda = 1.5416$ Å), in the 2θ range from 5° to 60°, with a step count of 3 s and a step size of 0.02° (2θ).

SEM. Surface morphology of materials was studied with a JEOL, JMS 6360LV with acceleration voltage of 20 kV. Microanalysis was conducted with energy dispersive X-ray spectroscopy (EDX) (Oxford Instruments, INCA Energy 200) coupled to SEM. nBG distribution in the composites was assessed by Silicon (Si) mapping.

Tensile mechanical test. Elastic modulus at 100% deformation (E_{100}), maximum tensile strength (σ_{max}), and maximum deformation (ε_{max}) were obtained after tensile test according to ASTM D882. For this, a Shimadzu AGSX with a cross head speed of 50 mm/min was used. Films of 33 mm long, 5 mm wide, 0.1 mm thick, and 25 mm of gauge length were used. Data were compared using one-way analysis of variance (ANOVA) with post hoc multiple comparison performed using Tukey's test. A minimum of $n = 5$ was used and $P < 0.05$ was considered significant.

In vitro bioactivity assays

The ability of the materials to induce the formation of apatite was evaluated by conditioning all samples in SBF #9 as described by Kokubo.[18] Circular samples

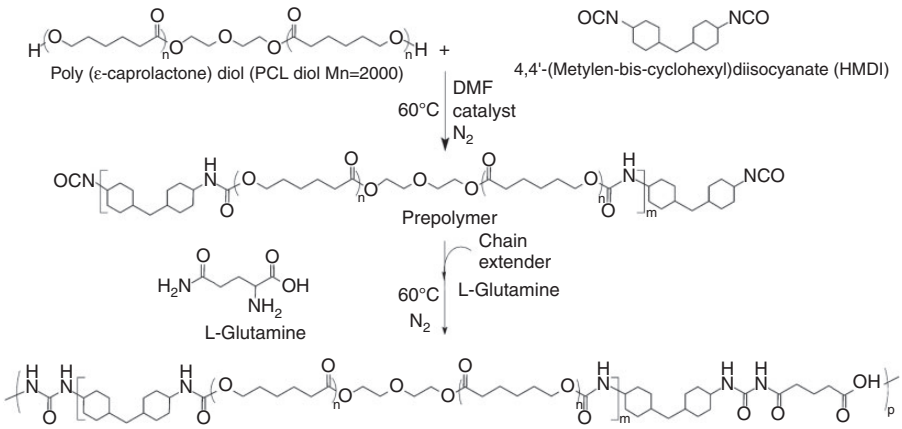

Figure 1. Suggested structure of segmented polyurethanes prepared with glutamine as chain extender (SPU-G).

of 11 mm diameter, three repeats for each time and material, were conditioned at 3, 7, and 10 days at 37°C in 20 ml of SBF as reported by others.[19] After this period of time, FTIR, SEM, EDX, and DRX were conducted as described above.

Cell culture

Stem cells isolated from dental pulp (DPSCs) were used to evaluate cell viability and differentiation in the presence of the materials. Approximately 6.5×10^3 cells were seeded on the materials and incubated at 37°C in a humidified air atmosphere containing 5% CO_2. The cell viability was evaluated using the 3-(4,5-dimethylthiazol-2-yl)5-(3-carboxymethoxyphenyl)-2-(4-sulfophenyl)-2H tetrazolium (MTS) assay according to the protocol provided by the manufacturer (CellTiter Aqueous One Solution cell proliferation assay kit from Promega). MTS assays were performed in quadruplicate after 2, 5, 7, and 9 days of cell culture. The osteogenic differentiation of DPSCs in the presence of the materials was evaluated by analyzing the Runx2 gene expression in basal culture medium for 48 h. Quantitative PCR was performed with the real-time PCR system, LightCyclerTM (Roche, Diagnostics, BS, SE).

Results and discussion

Properties of non-conditioned composites

Particle size distribution of nBG was ~120 nm, as obtained by DLS (Figure 2(b)), and this was confirmed by SEM at large magnifications (45,000×). SEM also showed an irregular morphology for the particles (Figure 2(a)). An acceptable distribution of nBG particles was observed, although nanoparticle clusters of nBG were detected, especially at high nBG concentrations.

SPU-G obtained from synthesis exhibited Mn and Mw of 28,966 g/mol and 77,649 g/mol, respectively. Neat SPU-G films were translucent but their composites become opaque as the concentration of nBG increased.

FTIR spectra of SPU neat films and composites are shown in Figure 3. In the unfilled polymer, absorption bands were observed at 3373 cm^{-1} corresponding to the N–H bond in the urethane/urea and at 2932 cm^{-1} and 2860 cm^{-1} those corresponding to the asymmetrical and symmetrical stretching vibration of CH_2 groups, from PCL, HMDI, and GLU. The carbonyl stretching (C = O) appeared between 1732 and 1760 cm^{-1} which includes the ester group from the PCL, and the urethane group (NHCOO). Amide II absorption (urethane N–H bending + C–N stretching)

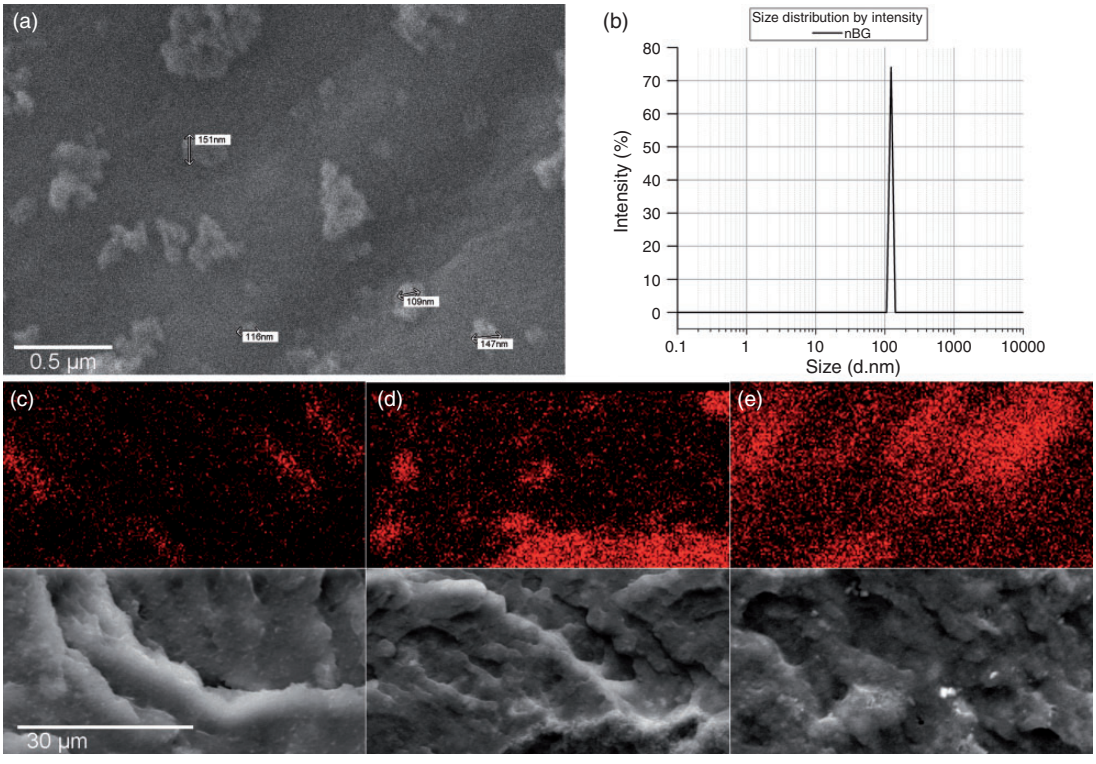

Figure 2. (a) SEM micrograph of nano BG particles, (b) particle size distribution of nBG by DLS. EDX mapping of Si (red), and corresponding SEM image of the cross-sectional area of composites with, (c) 5 wt.%, (d) 15 wt.%, and (e) 25 wt.% of nBG.

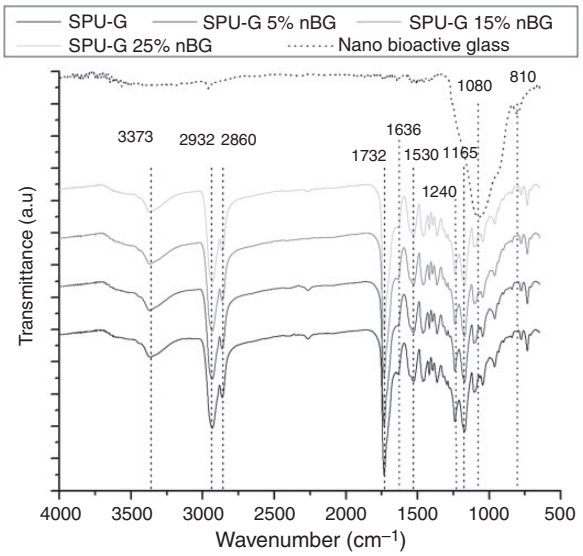

Figure 3. FTIR spectra of SPU-G, nBG, and SPU-G/nBG composites.

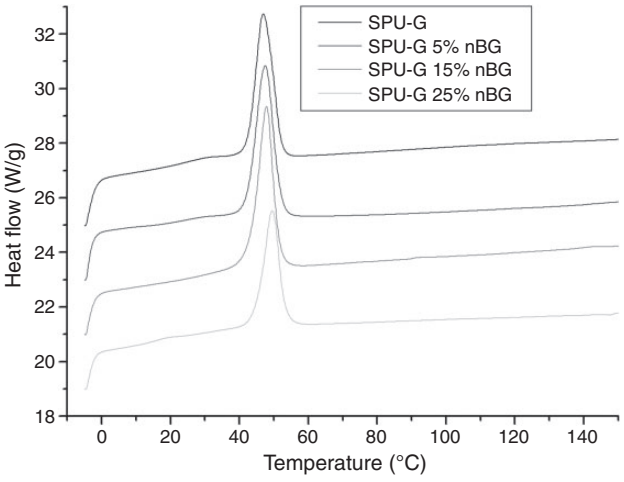

Figure 4. DSC thermograms of SPU-G and SPU-G/nBG composites.

was located at 1530 cm^{-1} and 1240 cm^{-1}, while the peak at 1165 cm^{-1} was attributed to the C–O–C stretching vibration in the soft segment. At 1636 cm^{-1} urea absorptions were detected.

In composites, infrared absorptions from the PU and the nBG were expected. Absorption bands were observed at 1080 cm^{-1} and 810 cm^{-1} corresponding to the symmetric vibration of Si–O–Si in the nBG.[9,10] These bands were expected to increase with nBG concentration but this was not observed in the composite probably because they were masked by the absorption characteristics of the PU, or because the amount of nBG at the surface was too low, as reported in similar studies of composites from PU and different fillers.[9,10,20]

DSC thermograms (Figure 4) showed a melting temperature (T_m) of 46°C for SPU-G, 47°C for composites with 5% and 15% of nBG, and 49°C for composites 25% of nBG. This suggests that the crystallinity of the PCL is not affected, at least on the first DSC trace, by the presence of bioactive glass.

TGA thermograms (Figure 5(a)) showed the main decomposition temperature (T_d) of the composites between 350° and 450°C. T_d of the composites increased as the concentration of nBG was increased. This is better seen in Figure 5(b) where the first derivative is plotted, and decomposition peaks are shifted to higher temperatures. It has been reported that the introduction of inorganic material nanoparticles into polymeric matrices can improve their thermal stability as the dispersed agents hinder the permeability of volatile degradation products out of the materials, i.e. the inorganic material generates a ''barrier effect'' which delays the release of thermal degradation products in comparison to the pristine polymer.[9,21–23]

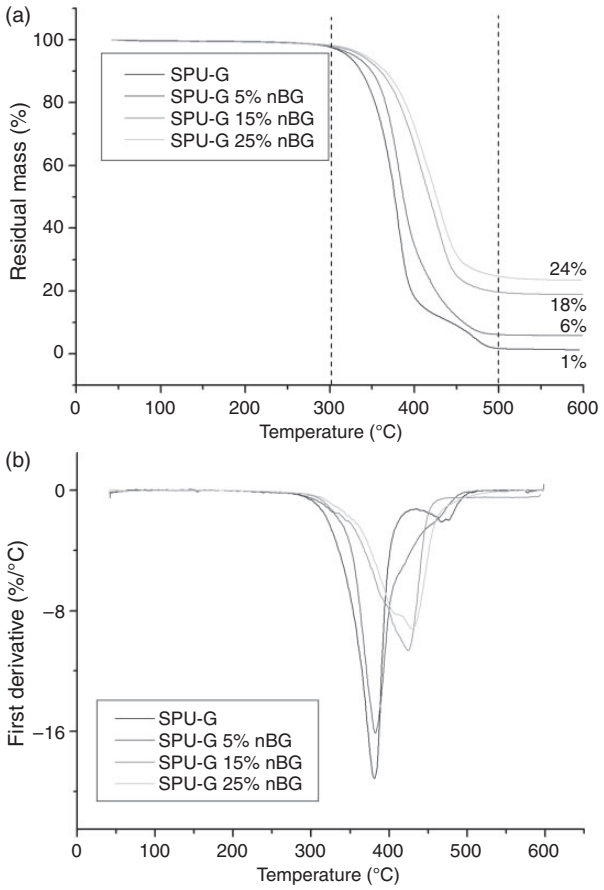

Figure 5. TGA thermograms of SPU-G and SPU-G/nBG composites. Residual mass (a) and first derivative of residual mass (b).

The maximum temperature used during thermogravimetric analysis was 650°C, which is far from the T_d of nBG (greater than 1100°C). As observed, the final mass was 24%, 18%, and 6% which is in close

Table 1. Elemental composition (weight %) of nBG, SPU-G, and SPU-G/nBG composites obtained by EDX.

	nBG	SPU-G	5%	15%	25%
C	11.5	67.3	63.7	59.4	64.9
O	49.6	32.7	34.7	37.6	35.0
Si	14.7	0	0.8	1.6	0.3
P	4.9	0	0.3	0.5	0.1
Ca	19.3	0	0.5	1.0	0.2

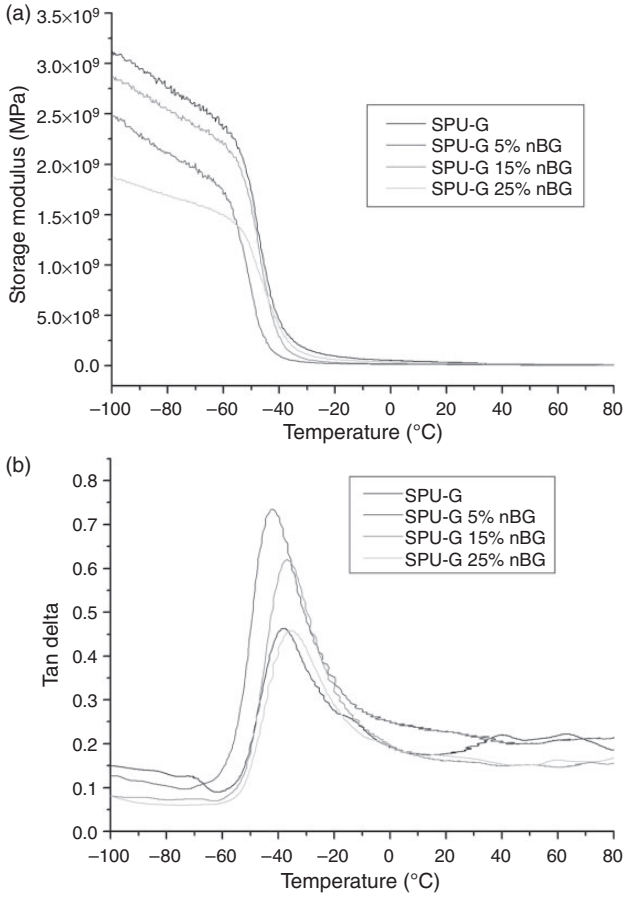

Figure 6. DMA thermograms of SPU-G and SPU-G/nBG composites. (a) storage modulus, and (b) tan delta.

agreement with the original composition of the composite. In addition, microanalysis performed on these composites showed that as the amount of nBG is increased in the composite, the amount of Si also increased (see Table 1). This was observed for 5% and 15% of nBG except for the composition of 25%, probably because of the heterogeneous surface distribution of the nBG.

Storage modulus (E′) and the dissipation factor (Tan δ) of each composite are shown in Figure 6 as obtained from the DMA thermograms. Figure 6(a) shows a significant

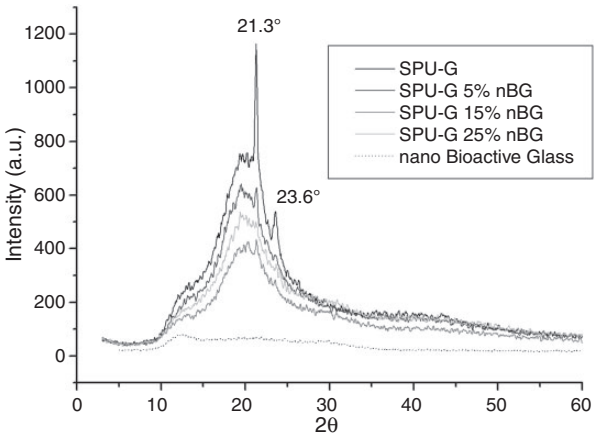

Figure 7. XRD patterns of SPU-G, nBG, and SPU-G/nBG composites.

drop in the storage modulus of the composite between −55° and −40°C. Furthermore, Figure 6(b) shows a peak in Tan δ, which can be associated to the T_g of the soft segments (PCL) of the PU.[5] For these composites, T_g slightly increased from −41 to −36°C as the amount of filler increased. The higher value of these transitions compared to pristine PCL ($T_g = -60$°C) suggests that the filler is restricting the movement of polymer chains.[21]

X-ray diffractograms of the composites are shown in Figure 7. Here, typical PCL reflections in the SPU-G are observed at 23.6° and 21.3° and in composites they become less intense and broad, as reported before.[5,10,17,24] As expected, nBG did not exhibit peaks due to its amorphous nature, in consequence composites only show peaks from the SPU-G matrix as reported for other systems.[12]

SEM images of composites are shown in Figure 8. The reported spherullitic morphology of PCL was not clearly observed in pure SPU-G films nor observed in any of the composites. Only a rough surface can be appreciated at all compositions.

Figure 9 shows the representative stress–strain curves obtained during the mechanical test of composites. Young's modulus, tensile strength, and maximum strain values are shown in Table 2. In general, tensile strength and deformation decreased significantly with nBG addition, i.e. from 22.2 to 12.2 MPa and 667.2 to 457.8%, respectively. However, Young's modulus did not show a significant difference between SPU and its composites.

Properties of composites after SBF conditioning

The formation of an apatitic layer covering the composites was expected as it is generally accepted when using bioactive glasses. This means that infrared absorption bands at 1032 cm^{-1} (PO_4^{3-}), at 875 and 1468 cm^{-1} (CO_3^{2-}) and 3565 cm^{-1} for hydroxyl group

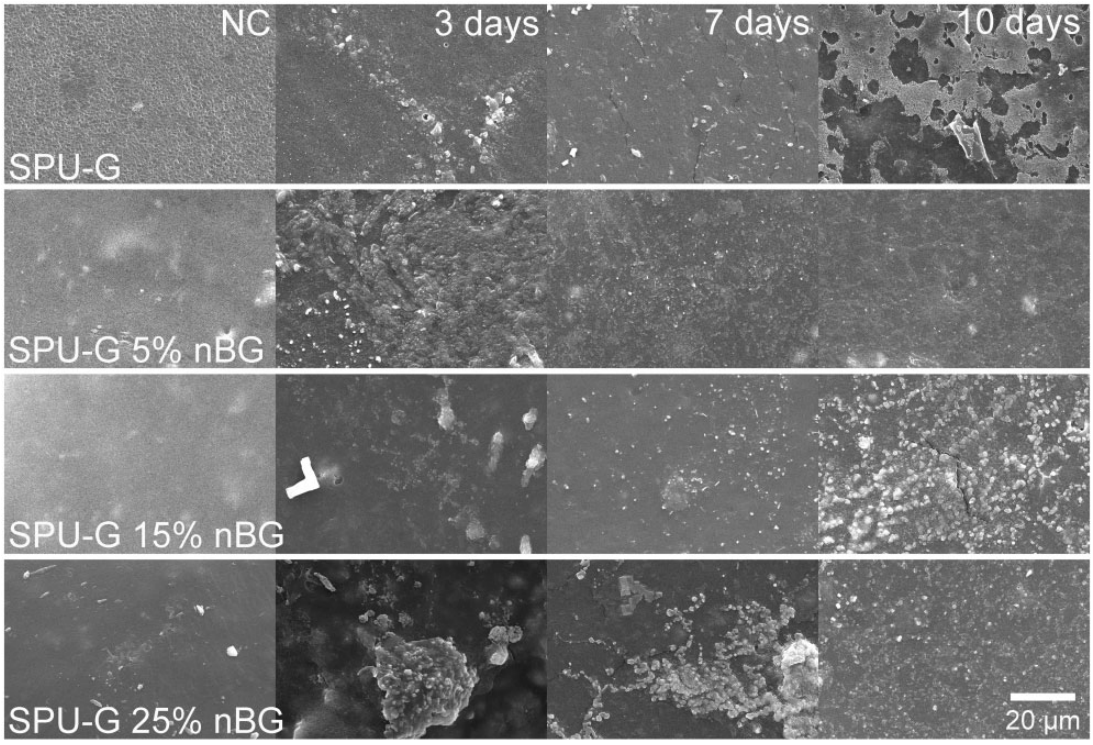

Figure 8. SEM micrographs of SPU-G and SPU-G/nBG composites non-conditioned (NC) and after conditioning in SBF for 3, 7, and 10 days.

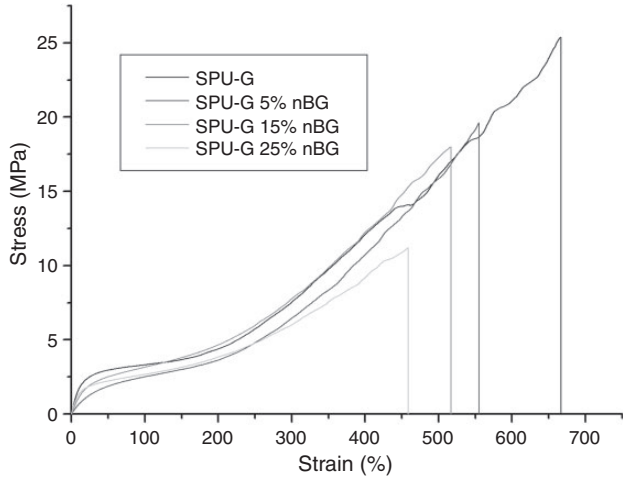

Figure 9. Tensile stress–strain curves of SPU-G and SPU-G/nBG composites.

(OH) should be observed. However, the infrared spectra of composite materials immersed in SBF even after 10 days only showed typical bands of PUs (see Figure 10). It has been reported that as earlier as 3 days, apatitic formation should occur but in our system even at day 10 no HA formation was detected. However, SEM images (Figure 8) showed deposits on the surface, which suggest the apatite layer formation.

Table 2. Tensile mechanical properties of pure SPU-G and SPU-G/nBG composites.

	E_{100} (MPa)	σ_{max} (MPa)	ε_{max} (%)
SPU-G	3.21 ± 0.58	22.42 ± 5.90	667.21 ± 74.36
SPU-G 5% nBG	2.58 ± 0.05	20.89 ± 3.91	555.30 ± 34.84
SPU-G 15% nBG	2.92 ± 0.15	17.35 ± 3.87	516.79 ± 46.21
SPU-G 25% nBG	2.94 ± 0.31	12.08 ± 1.84	457.85 ± 33.09

This apparent contradiction can be easily explained if one considers the depth analyzed by ATR-FTIR technique. The agglomerates were more evident at higher concentrations of nBG and longer conditioning times, as reported on literature.[9–11]

In order to confirm the composition of these deposits, elemental analysis was performed by means of EDX. However, the presence of calcium (Ca) and phosphorus (P) alone cannot be used as evidence of the formation of the apatite layer[20] as these elements are present in the nBG (Ca/P = 2.94 (atomic%) or Ca/P = 3.07 (wt.%)). It can be seen in Table 3 that the Ca/P ratio for stoichiometric HA (1.67) was not achieved in any of these composites as a Ca/P ratio close to 1 was observed. This may suggest that other calcium phosphates such as amorphous calcium phosphate (ACP) (Ca/P = 1.2 – 2.2) or brushite (DCPD) (Ca/P = 1) are formed,[25] explained

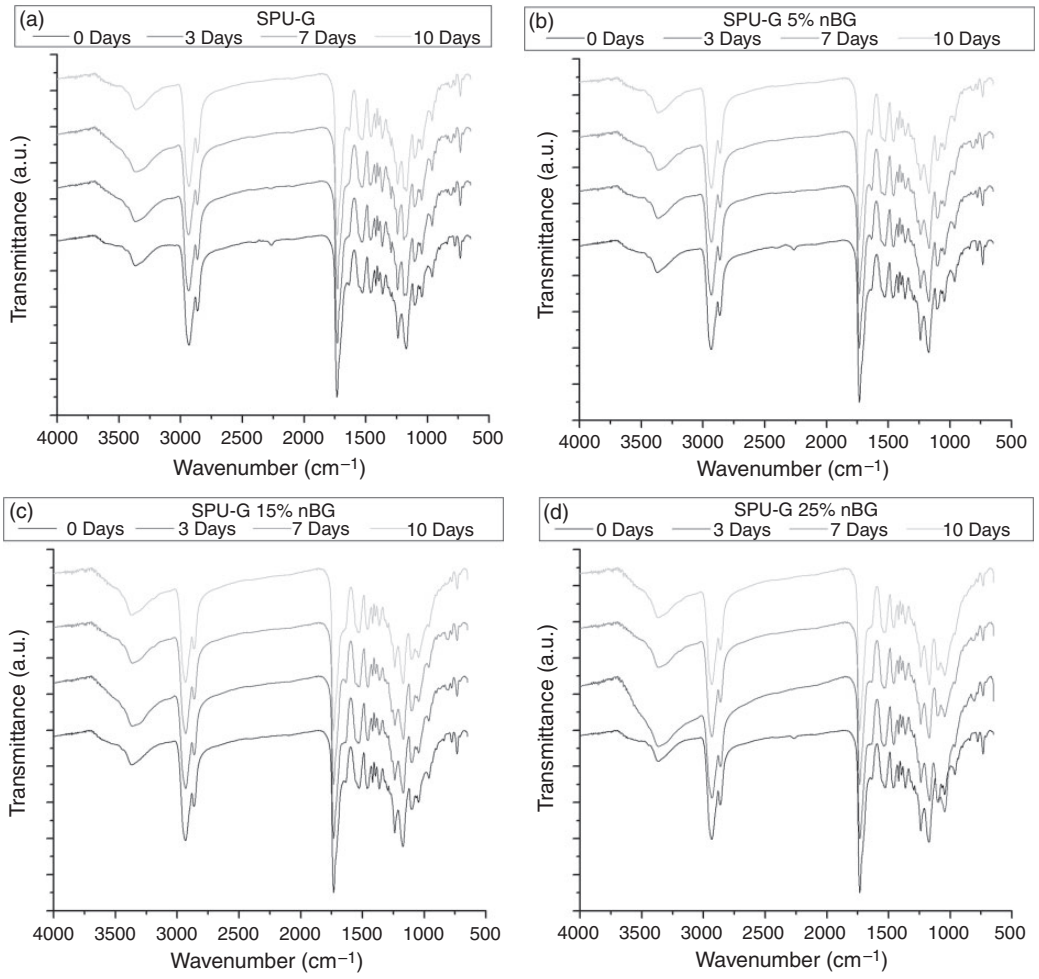

Figure 10. FTIR spectra of composites conditioned at 3, 7, and 10 days in SBF at 37°C; SPU-G (a), SPU-G 5% nBG (b), SPU-G 15% nBG (c), and SPU-G 25% nBG (d).

by heterogeneous deposits on the analyzed zones of materials.

Further confirmation of the structure of calcium deposits came from XRD analysis (see Figure 11). Peak corresponding to an apatitic layer can be located at 31.9°.[18,24,26] This reflection was observed almost in all composites after conditioning in SBF, even at three days conditioning. In addition to this main peak, a second reflection was observed at 29.4° in the 5 wt.% composites after three days of conditioning, and in the 15 wt.% after three and seven days, and in the 25 wt.% after three days. This can be related to formation of ACP, DCDP, calcite, or calcium carbonate.[11,25] Other peaks associated to the formation of apatitic layer or HA on these composites were observed at 25.9°, 26°, 32.7°, 34.6°, 36.7°, 49.6°, and 50.4° as reported in other studies.[12,17,24–27]

Biological properties of composites

The use of silicate based bioactive glasses is reported to promote osteoblast adhesion and proliferation.[28] In our study, MTS assay showed that DPSC proliferation initially increased (up to day 5) for all composition studied. However, it was compromised at day 9 when composites contained high contents of nBG (Figure 12). Cell proliferation increased at day 9 in composites containing up to 2.5% of nBG, possibly because the concentration of ions in the medium increases with time. At day 9, cells are dead in composites with higher nBG concentrations because the excessive alkalinization produced by ion exchange between the glass and the medium.

The Runx2 expression is comparable between different compositions, except for the 15% and 25% nBG composites (Figure 13). In the later composites, Runx2 was overexpressed as more Ca^{2+}, PO_4^{3-} or even silicon are released, inducing cell differentiation.

At 48 h, cell proliferation and Runx2 expression are balanced but this early marker of osteogenic differentiation was not assessed on the same day of the studied proliferation and therefore it is not possible to correlate both parameters. Although it is desirable to study this

Table 3. Calcium/phosphorous ratio of SPU-G/nBG composites after conditioning in SBF at 37°C, obtained by EDX.

	Composite	Ca/P (weight %)	Ca/P (atom %)
Not conditioned	BG	2.94	3.07
	SPU-G	(P = 0)	(P = 0)
	SPU-G 5% nBG	2.13	1.64
	SPU-G 15% nBG	1.96	1.50
	SPU-G 25% nBG	(P = 0)	(P = 0)
3 days	SPU-G	(P = 0)	(P = 0)
	SPU-G 5% nBG	1.08	0.83
	SPU-G 15% nBG	0.92	0.71
	SPU-G 25% nBG	1.18	0.91
7 days	SPU-G	(P = 0)	(P = 0)
	SPU-G 5% nBG	1.10	0.78
	SPU-G 15% nBG	1.61	1.30
	SPU-G 25% nBG	1.03	0.71
10 days	SPU-G	(P = 0)	(P = 0)
	SPU-G 5% nBG	0.93	0.75
	SPU-G 15% nBG	0.90	0.64
	SPU-G 25% nBG	0.83	0.70

marker for a longer time,[29] there are some reports where Runx2 expression is studied only at one time point.[30] Thus, the incorporation of appropriate

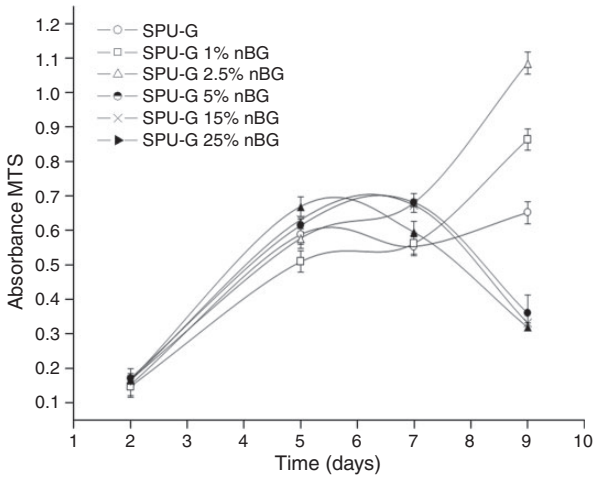

Figure 12. Viability of DPSCs cultured in the presence of the SPU-G/nBG composites at different culture times as determined by the MTS assay.

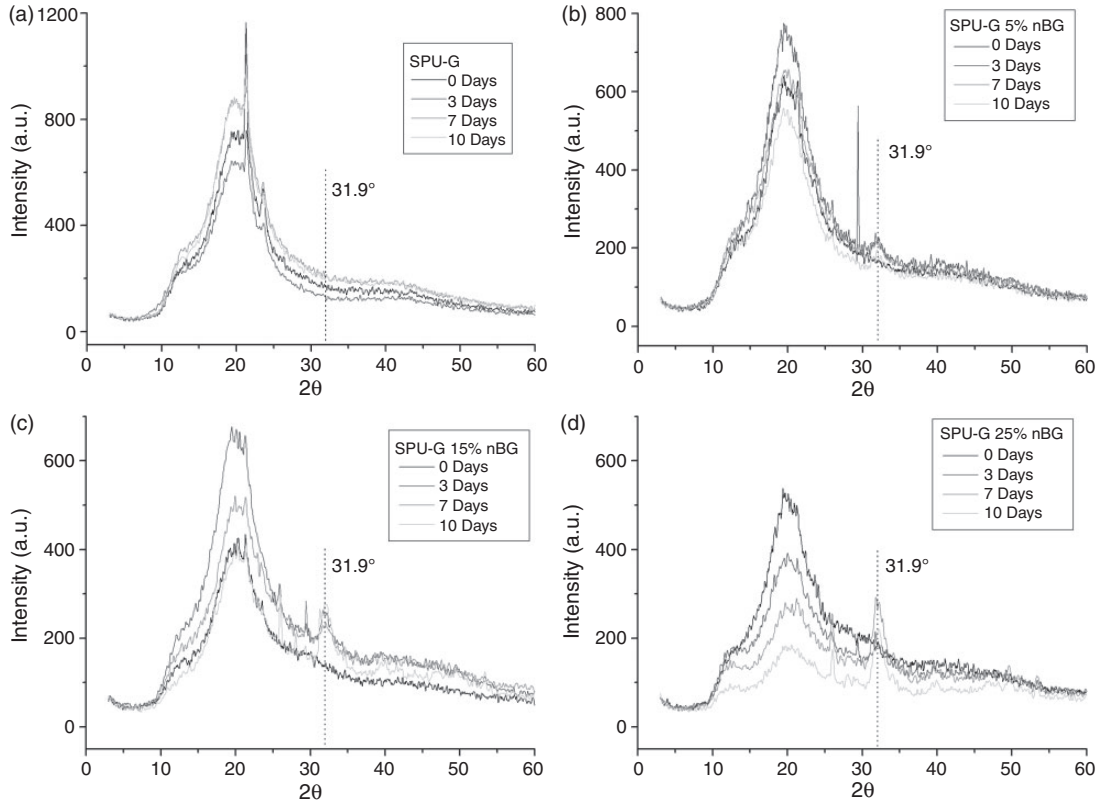

Figure 11. XRD patterns of composites conditioned at 3, 7, and 10 days in SBF at 37°C; SPU-G (a), SPU-G 5% nBG (b), SPU-G 15% nBG (c), and SPU-G 25% nBG (d).

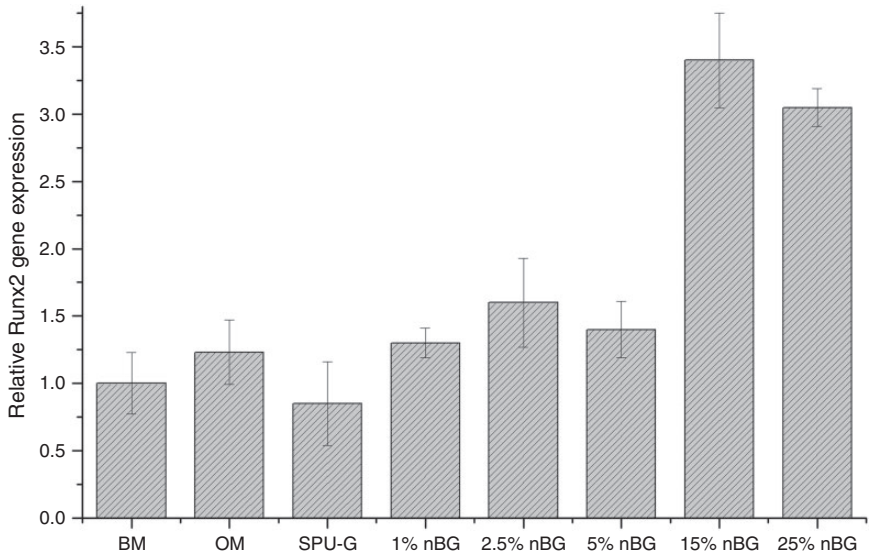

Figure 13. Relative Runx2 expression in DPSCs cultured for 48 h with SPU-G/nBG composites in the absence of osteogenic supplements.

contents of nBG into the PU matrix can be used to provide it osteostimulative properties.

Conclusions

SPU-G/nBG composites combine the good properties of both materials when used separately. The brittle nature of nBG was improved by its incorporation into a polymeric matrix of poor biocompatibility. In this manner, semycrystalline elastomeric composites with good mechanical properties were obtained for instance with 5 wt.% of nBG. However, at 15 or 25 wt.%, their mechanical performance was compromised. In spite of this, they showed good mineralization potential. The in vitro mineralization test using SBF showed the formation of deposits of varying composition including calcium phosphates, calcium carbonates, and apatite in most cases. These calcium derivatives were more evident when the content of nBG was higher and after extended times of conditioning in SBF. In addition, nBG composites were also able to induce the osteogenic differentiation of DPSCs. These properties render them suitable for guided bone regeneration, for example, in the maxillary bone, where osteoconductivity is desirable but not a demanding mechanical performance.

Declaration of Conflicting Interests

The author(s) declared no potential conflicts of interest with respect to the research, authorship, and/or publication of this article.

Funding

The author(s) disclosed receipt of the following financial support for the research, authorship, and/or publication of this article: The authors thank CONACYT and CONICYT for the Mexico-Chile Bilateral Cooperation Project 208518. The authors also thank Patricia Quintana and Daniel Aguilar Treviño for XRD experiments at Laboratorio Nacional de Nano y Biomateriales (LANBIO), Cinvestav-IPN, Unidad Mérida (Projects FOMIX-Yucatan 2008-108160 and CONACYT LAB-2009-01 no. 123913).

References

1. Jacob S. Global prevalence of periodontitis: a literarure review. *Int Arab J Dent* 2012; 3: 26–30.
2. Brydone AS, Meek D and Maclaine S. Bone grafting, orthopaedic biomaterials, and the clinical need for bone engineering. *Proc Inst Mech Eng Part H* 2010; 224: 1329–1343.
3. Mumford JE and Simpson AHRW. Management of bone defects a review of available techniques. *lowa Orthop J* 1992; 12: 42–49.
4. Jones JR and Lee PD. Bioactive glass scaffolds with hierarchical structure and their 3D characterization. *Key Eng Mater* 2010; 441: 123–137.
5. Chan-Chan LH, Solis-Correa R, Vargas-Coronado RF, et al. Degradation studies on segmented polyurethanes prepared with HMDI, PCL and different chain extenders. *Acta Biomater* 2010; 6: 2035–2044.
6. Kavlock KD, Pechar TW, Hollinger JO, et al. Synthesis and characterization of segmented poly(esterurethane urea) elastomers for bone tissue engineering. *Acta Biomater* 2007; 3: 475–484.
7. Wang L, Li Y, Zuo Y, et al. Porous bioactive scaffold of aliphatic polyurethane and hydroxyapatite for tissue regeneration. *Biomed Mater* 2009; 4: 025003.
8. Bonzani IC, Adhikari R, Houshyar S, et al. Synthesis of two-component injectable polyurethanes for bone tissue engineering. *Biomaterials* 2007; 28: 423–433.
9. Ryszkowska JL, Auguścik M, Sheikh A, et al. Biodegradable polyurethane composite scaffolds

containing Bioglass® for bone tissue engineering. *Compos Sci Technol* 2010; 70: 1894–1908.
10. de Oliveira AAR, de Carvalho SM, Leite MDF, et al. Development of biodegradable polyurethane and bioactive glass nanoparticles scaffolds for bone tissue engineering applications. *J Biomed Mater Res B Appl Biomater* 2012; 100: 1387–1396.
11. Deb S, Mandegaran R and Di Silvio L. A porous scaffold for bone tissue engineering/45S5 Bioglass derived porous scaffolds for co-culturing osteoblasts and endothelial cells. *J Mater Sci Mater Med* 2010; 21: 893–905.
12. Valenzuela F, Covarrubias C, Martínez C, et al. Preparation and bioactive properties of novel bone-repair bionanocomposites based on hydroxyapatite and bioactive glass nanoparticles. *J Biomed Mater Res B Appl Biomater* 2012; 100: 1672–1682.
13. Hench LL, Xynos ID and Polak JM. Bioactive glasses for in situ tissue regeneration. *J Biomater Sci Polym Ed* 2004; 15: 543–562.
14. Bellucci D, Chiellini F, Ciardelli G, et al. Processing and characterization of innovative scaffolds for bone tissue engineering. *J Mater Sci Mater Med* 2012; 23: 1397–1409.
15. Su J, Cao L, Yu B, et al. Composite scaffolds of mesoporous bioactive glass and polyamide for bone repair. *Int J Nanomedicine* 2012; 7: 2547–2555.
16. Covarrubias C, Arroyo F, Balanda C, et al. In vitro bioactivity and cell differentiation properties of nanobioceramics with different nanostructure. In: *26th Annual conference of the European society for biomaterials*, Liverpool, UK, 31 August–3 September 2014.
17. Cetina-Diaz SM, Chan-Chan LH, Vargas-Coronado RF, et al. Physicochemical characterization of segmented polyurethanes prepared with glutamine or ascorbic acid as chain extenders and their hydroxyapatite composites. *J Mater Chem B* 2014; 2: 1966–1976.
18. Kokubo T and Takadama H. How useful is SBF in predicting in vivo bone bioactivity? *Biomaterials* 2006; 27: 2907–2915.
19. Navarro M and Planell JA. Bioactive composites based on calcium phosphates for bone regeneration. *Key Eng Mater* 2010; 441: 203–233.
20. Asefnejad A, Behnamghader A, Khorasani MT, et al. Polyurethane/fluor-hydroxyapatite nanocomposite scaffolds for bone tissue engineering. Part I: morphological, physical, and mechanical characterization. *Int J Nanomedicine* 2011; 6: 93–100.
21. Cervantes-Uc JM, Moo-Espinosa JI, Cauich-Rodríguez JV, et al. TGA/FTIR studies of segmented aliphatic polyurethanes and their nanocomposites prepared with commercial montmorillonites. *Polym Degrad Stab* 2009; 94: 1666–1677.
22. Zhang Y, Xia Z, Huang H, et al. Thermal degradation of polyurethane based on IPDI. *J Anal Appl Pyrolysis* 2009; 84: 89–94.
23. Cauich-Rodríguez JV, Chan-Chan LH, Hernandez-Sánchez F, et al. Degradation of polyurethanes for cardiovascular applications. In: Rosario P (ed.) *Advances in Biomaterials Science and Biomedical Applications*. Rijeka, Croatia: InTech, 2013, pp.51–82.
24. Dong Z, Li Y and Zou Q. Degradation and biocompatibility of porous nano-hydroxyapatite/polyurethane composite scaffold for bone tissue engineering. *Appl Surf Sci* 2009; 255: 6087–6091.
25. Dorozhkin SV. Calcium orthophosphates. *J Mater Sci Mater Med* 2007; 42: 1335–1363.
26. Katsanevakis E, Wen XJ, Shi DL, et al. Biomineralization of polymer scaffolds. *Key Eng Mater* 2010; 441: 269–295.
27. Cisneros-Pineda OG, Herrera Kao W, Loría-Bastarrachea MI, et al. Towards optimization of the silanization process of hydroxyapatite for its use in bone cement formulations. *Mater Sci Eng C* 2014; 40: 157–163.
28. Lopes P, Garcia M, Fernandes M, et al. Properties and osteoblast cytocompatibility of self-curing acrylic cements modified by glass fillers. *J Biomater Appl* 2013; 28: 498–513.
29. Phillips JE, Gersbach CA, Wojtowicz AM, et al. Glucocorticoid-induced osteogenesis is negatively regulated by Runx2/Cbfa1 serine phosphorylation. *J Cell Sci* 2006; 119: 581–591.
30. Covarrubias C, Arroyo F, Balanda C, et al. The effect of the nanoscale structure of nanobioceramics on their in vitro bioactivity and cell differentiation properties. *J Nanomater* 2015; 2015: 1–14.